FYP

Donovan Webb

Department of Physics, University of Bath, Bath BA2 7AY, United Kingdom

E-mail: dw711@bath.ac.uk

Abstract.

XXPREVIOUSXX A device capable of uniformly concentrating a magnetic fields inside of a free space cavity will increase the efficiency of many magnetic devices and sensors. This project shall look at a proposed design for a magnetic field concentrator informed by the transformation optic technique. A metamaterial shell comprised of high and low permeability sections alternating in the angular direction has been shown to approximate the designed concentrator[**?**]. The ability of the shell acting as a concentrator will be explored in various regimes with a specific focus on improving efficiency of wireless power transmission.

1. Introduction

The manipulation of magnetic fields is a critical tool for many modern technologies. Magnetic devices often have efficiencies dependent on the strength of interaction with an external magnetic field. Examples include energy harvesting from magnetic fields [**?**] to brain activity scans by locating small magnetic gradients [**?**]. These devices may have increased efficiency by concentrating the desired magnetic field within the area of sensing or harvesting.

Magnetic fields may be described by Maxwell's equations [**?**] and are guided by materials due to their optical properties, such as permitivity and permeability [**?**]. Fermat's principle of least time allowed the design of many optical devices using geometrical lenses [**?**], however, with the maturation of fabrication techniques, many materials may be produced with exotic anisotropic optical properties [**?**] prompting the development of transformation optics (TO) — a modern approach to optical device design.

Here we describe one such TO designed device; The magnetic concentrator [**?**], with a particular focus on its efficacy in wireless power transmission.

1.1. Transformation Optics and Metamaterials

TO informed the design of many new devices such as perfect lenses [], magenetic-hoses [], -cloaks [], -rotators [], -blackholes [], and -concentrators []. It can be shown that due to the form invariance of Maxwell's equations, a spatial coordinate transform is equivalent to the insertion of a material with specific permeabilities and permitivities. This is shown conceptually by the three steps of the schematic shown in figure 1. First a ray is considered in free cartesian space in panel a, which due to Fermat's principle of least time will be following the horizontal spatial grid lines. The space is then transformed arbitrarily in panel b so that the ray adopts the desired path for the final device. The transformation required, A, to morph the ray now informs the optical properties for the specific inserted material of panel c, which is once again located in untransformed space.

The form invariance of Faraday's law is described by the equivalent expressions

$$\nabla' \times \mathbf{E'} = -jw[\mu_0]\mathbf{H'} \qquad and \qquad \nabla \times \mathbf{E} = -jw[\mu']\mathbf{H}, \tag{1}$$

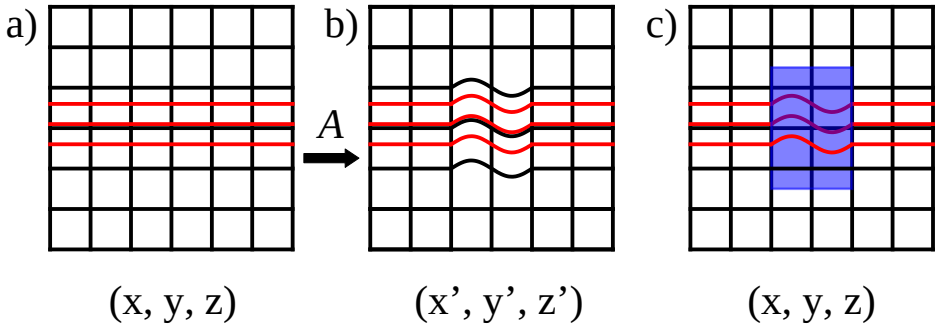

Figure 1. The steps of Transformation Optics. a) A ray (red) travelling in untransformed spatial coordinates (black grid) follows the path of least time. b) A spatial coordinate transformation A is applied to guide the ray along a desired path. c) A material (blue) is insterted into the untransformed space with corresponding permeability and permitivity which mimics the spatial coordinate transform A for the ray.

where the first is expressed in transformed coordinate space $x'(x,y,z), y'(x,y,z), z'(x,y,z)$ and free space permeability $[\mu_0]$, whilst the second is expressed in untransformed cartesian space x, y, z but with some space dependent permeability $[\mu']$. Similar equivalent expressions exist for the other Maxwell equations but with some non-free permittivity $[\epsilon']$.
The required permeability and permittivity is found by,

$$\mu' = \frac{A\mu_0 A^T}{|A|} \qquad and \qquad \epsilon' = \frac{A\epsilon_0 A^T}{|A|} \tag{2}$$

where A is the Jacobian matrix describing the transformation of coordinate systems (e.g. between panel a and panel b in figure 1).
The resulting calculated optical properties may be anisotropic, have arbitrary magnitude and even be negative []. As bulk materials rarely, if ever, show these properties, optical metamaterials are often required [**?**].
Metamaterials are often comprised of repeating units whose dimensions are much smaller than the wavelength of the interacting radiation [**?**]. The individual units may have specific geometery, orientation and optical properties to selectively interact with incident waves so that the net effect of the material mimics a bulk substance with different optical properties than its substituent parts.

1.2. Magnetic Concentrator

As described above, a device capable of magnetic field concentration can increase the efficiency of sensors and energy harvesters. Utilising TO we may design an optimal field concentrator which fulfils the criteria: All magnetic field within a region A is confined to region B where B is free space only. A possible geometry for this device that has cylindrical symmetry is shown in XfXfigure **??**. A ray diagram is shown in XfXfigure **??** for free space with no inserted material. Two coordinate transforms are now applied: First the region $\rho < R_2 - \eta$ is radially and linearly compressed to the region $\rho < R_1$; Second, to ensure the continuity of our transformed space, a high (k^{th}) order polynomial radial expansion of $R_2 - \eta < \rho < R_2$ to the region $R_1 < \rho < R_2$ is made. These transformations are described by the coordinate transformations,

$$\begin{aligned} \rho' &= \frac{R_1}{R_2 - \xi}\rho, & \rho' &\in [0,\ R_2 - \xi) \\ \rho' &= R_2^{1-k}\rho^k & \rho' &\in [R_2 - \xi,\ R_2). \end{aligned} \tag{3}$$

By symmetry we see that θ and z remain unchanged through the two transformations. The corresponding Jacobians may be found for these transformations and using equation 2, the permeabilities of the required inserted material may be found to be

$$\begin{aligned} \mu' &= \begin{pmatrix} 1 & 0 & 0 \\ 0 & 1 & 0 \\ 0 & 0 & (\frac{R_2-\xi}{R_1})^2 \end{pmatrix} && \rho' \in [0,\ R_1) \\ \mu' &= \begin{pmatrix} k & 0 & 0 \\ 0 & 1/k & 0 \\ 0 & 0 & \frac{1}{k}(\frac{\rho'}{R_2})^{2/k-2} \end{pmatrix} && \rho' \in [R_1,\ R_2) \end{aligned} \tag{4}$$

Taking the limit $\eta \to 0$ in order to concentrate all of the field within A into B, and matching the boundary conditions at $R_2 - \eta$ and at $R1$, we find that $k \to \infty$. From this we find that the required permeability within B is satisfied by free space whilst a material with radial permeability $\mu_\rho \to \infty$ and angular permeability $\mu_\theta \to 0$ is required for region A. The z components of permeability is ignored as we assume it to be invariant if the cyclindrical shell is significantly extended in the z direction.
To satisfy this highly anisotropic condition, an exploration of metamaterials is required. A possible discretized shell construction is proposed [**?**] where the high radial permeability is provided by ferromagnetic materials whilst the angular permeability is shielded by superconducting material. Materials such as MuMetal, have relative permeabilities of up to XvX [**?**] and ideal superconductors in their Meissner state will exclude all magenetic fields from within their interior giving a relative permeability of 0 [**?**]. These two materials may be arranged in alternating angular sheets, as seen in figure **??**, to approximate the conditions proposed by TO design.
XeX discuss where this concentration originates?
In an external static uniform magnetic field, the ideal shell will increase the field within region B by a factor of R_2/R_1. Similarly if a dipole with magnetic moment m is present at the origin and surrounded by the magnetic concentrator shell, then the field outside of the shell will be increased by a factor of R_2/R_1. Therefore for an observer at $\rho > R_2$ it will appear that a dipole with magnetic moment $m \cdot R_2/R_1$ is present at the origin.

(Comparison to other conc. techniques: It is known that ferromagnetic materials concentrate magnetic fields within their bulk [**?**] however, concentration of the field into a free space cavity may be required.)

1.3. Wireless Power Transfer

The ability to transfer power between devices that are not connected by wires is useful in many settings: for convenince, e.g. mobile phones; for safety, e.g. implanted medical devices; or for practicallity, e.g. satellites. We shall focus on near field power transmission by the use of inductive coupling. Inductive coupling transfers power between two coils of wire by an oscillating magnetic field as seen in figure 2 *a*. The transmitting coil is supplied with an alternating current, which by Ampere's law creates an oscillating magnetic field. The receiving coil is placed within this magnetic field, so that a current is induced as described by Faraday's law. This strategy for power transfer is highly sensitive to distance as the magnetic field of a dipole drops off with distance cubed, r^{-3}, therefore the power is proportional to r^{-6}. The overall efficiency therefore suffers with distance as the non-ideal resistive losses in the primary coil remain (relatively) constant with distance. To somewhat counteract this sharp drop off of efficiency with distance, concentrating shells may be used to magnify the transmitted field and locally concentrate the field around the receiving solenoid. The concentrating shell is larger than the coil by necessity however the presence of a shell is always advantageous when the free space

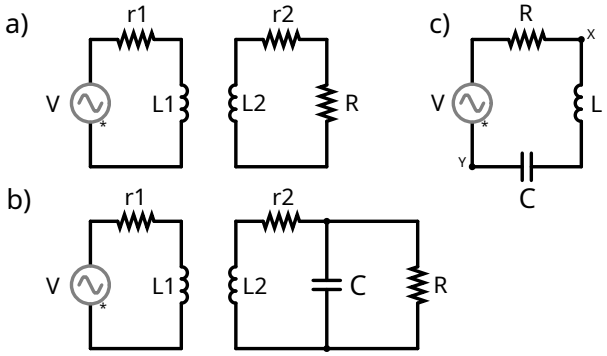

Figure 2. Wireless power transmission by inductive coupling. a) Simple circuitary for coupling $L1$ and $L2$ coils. The useful power transmitted is across load resistance R whilst power lost is internal resistance of coils, $r1$ and $r2$. b) The receiving inductor is now part of a resonant RLC circuit. c) A series RLC circuit — when voltage at x and y are in phase, the resonant condition is met.

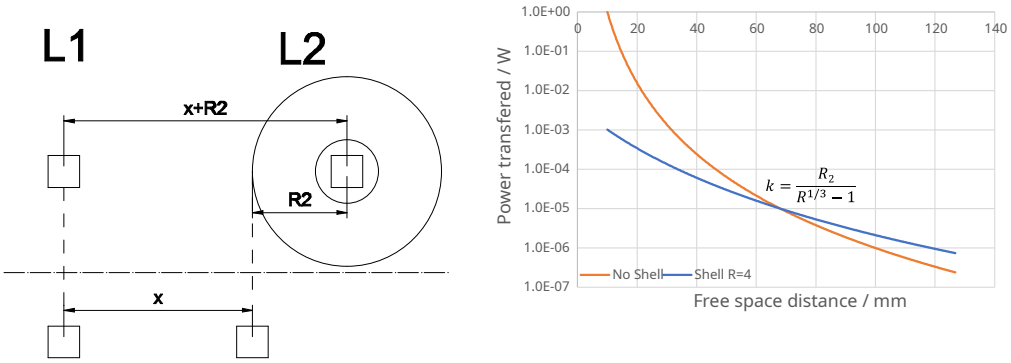

Figure 3. Wireless power transmission by inductive coupling is proportional to r^{-6}. A concentrating shell increases this power transfer by $(R_2/R_1)^2$ but at the cost of less free space, x, between the devices. However, at a critical distance k, the shell provides an improvement over bare dipoles for a given free space distance, x. LHS: The arrangement of two dipoles (boxes) L_1 and L_2 with a fixed free space gap x, either with a shell (Top) or without (Bottom). RHS: Theoretical power transfer plots for these two arrangements when the shell has $R_2 = 40$ mm, $R_1 = 10$ mm.

distance between the power transmitting and power receiving device is greater than k, where

$$k = \frac{R_2}{\sqrt[3]{R} - 1} \tag{5}$$

and R is the ratio R_2/R_1. This arrangement and the critical distance k is shown in figure 3.

2. Methods

2.1. Construction of shell

$0.X$ mm MuMetal XXX and $0.X$ mm copper was cut into X by X rectangular sheets. A plastic support for holding the MuMetal and Copper sheets was 3D printed using an ultimaker XX to produce

the shells seen in figure **??**, with an R_2/R_1 ratio of XXX.

2.2. DC Magnetic Fields

Helmholtz coils were powered by a constant DC current to create a uniform magnetic field within their center. A commercially available XXX Hall probe was zeroed by using a MuMetal cannister, and then placed at the center of the Helmholtz coils. A Hall probe relates a measured Hall voltage, V_H, to a surrounding magnetic field, B [**?**] as

$$V_H = \frac{IB}{net}. \tag{6}$$

The probe maintains constant current supply I, and material paramaters n (charge carrier density), e (charge of electron) and t (thickness of probe) meaning a calibrated probe may give accurate readings for magnetic fields.
The magnetic field, B, produced at the center of Helmholtz coils with radius R, seperated by a distance R should follow,

$$B = \frac{8}{5\sqrt{5}}\frac{\mu_0 nI}{R}, \tag{7}$$

where I is the current supplied to the coils and n is the number of turns of wire. This equation follows directly from the Biot-Savart law [**?**] and the relative geometry of the coils as seen in figure **??**. From equation 7 it can be seen that the magnetic field should increase linearly with supplied current. Using the Hall probe we ensured this was the case and found the relationship of current supplied to magnetic field produced for our paticular Helmholtz arrangement.
Now, with the capability to produce known external magnetic fields, the described field concentrating shells may be placed within this field and the Hall probe may be placed within their inner radius to measure concentrated field.

2.3. AC characterization

Use of solenoid, limitations due to pick up.
Due to the induced voltage across the inductor being small and background noise being high, a lock-in amplifier was used to select only the desired signal frequency. This substantially reduced noise in our readings allowing higher frequency and lower magnetic field strength experiments.

2.4. Power Transfer

Power transfer experiments measure power dropped across a load resistor in a receiving circuit versus power lost in the transmitting circuit's inductor. The receiving circuit, seen in figure 2, has multiple arrangements to optimise power transfer, the simplest of which is the load resistor in series with the receiving inductor forming an RL circuit. If at the operating frequency, ω, the non-ideal real resistances of the coil, is assumed to be $r_2 << \omega L$, then the optimal load resistance for power transfer is found as,

$$\begin{aligned} V_s &= I_s(j\omega L_2 + R), \\ P_s &= |I_s|^2 R = \frac{V_s^2 R}{\omega^2 L_2^2 + R^2}, \end{aligned} \tag{8}$$

and by differentiating, we find a maxima occurs in P_s occurs at

$$R = \omega L_2. \tag{9}$$

The EMF induced in the receiving coil of a coupled inductance system may be found by Faraday's law,

$$\varepsilon = -\frac{d\phi_{21}}{dt}, \tag{10}$$

where ϕ_{21} is the magnetic flux through coil 2 due to the current of coil 1. By defining a mutual inductance between two coils as,

$$M = \frac{\phi_{21}}{I_1}, \tag{11}$$

we find the equivalent expression for Faraday's law,

$$\varepsilon = -M\frac{dI_1}{dt}. \tag{12}$$

If the current in coil 1 is alternating sinuisoidally, then the maximum EMF induced in coil 2 will be $MI_1\omega$. Changes in mutual inductance for different shell constructions is a useful metric for field concentration as it is proportional to the magnetic flux present in coil 2. It may also be readily calculated if current in coil one is known and the voltage across the load resistance in circuit 2 is measured when $R = \omega L$ as,

$$V_s = \frac{MI_1\omega}{\sqrt{2}}. \tag{13}$$

To maximise power transfer an RLC circuit is constructed on the receiving circuit. Ideally in an RLC circuit the complex impedance of the inductance and capacitance cancel leaving only the load resistance. Our inductance is set by the solenoid we chose to use and so for exploring power transfer at various frequencies, a capacitance can be found to satisfy the resonance condition. If inductance, L, does not vary then capacitance, C, is easily found by,

$$C = \frac{1}{w^2 L}. \tag{14}$$

However, we need not assume that inductance is constant. A series RLC circuit can be constructed as seen in figure 2 *c* to ensure resonance is met. Resonance occurs in this circuit when V_x is exactly in phase with V_y. In this case any imaginary impedances are cancelled and only real resistance remains. For maximal power transfer a parallel RLC circuit is preferable however due to the restraints of the experiement a non-ideal version must be made as seen in figure 2 *b*. The resonant condition found by the series RLC is a close approximation to this more complicated parallel circuit.
To maximise power transfer in the series RLC case, a familiar idea of impedance matching occurs, i.e. Power is maximised when the load resistance is equal to any internal resistances of the components [**?**]. As internal resistances are difficult to measure and may depend on current XXX, this could also be found experimentally by measuring voltage and current over the load resistance whilst varying load resistance.
For the parallel RLC case, a more complicated expression for optimal load resistance was found which depends non trivially on a combination of internal resistances. A model is proposed below, however, experimentally locating the optimal resistances was chosen as measuring internal resistances proved difficult and time consuming.
XXTheory of Rload dependence on power transfer.

3. Results

3.1. DC Magnetic Fields

Using the DC Helmholtz set up as described in Methods, we observed constant concentration factors for different shell constructions in an external magnetic field ranging from 1 G to 22 G. No shell, 18 MuMetal, 36 MuMetal, 18 Copper and 18 MuMetal + 18 Copper shells were used and their concentration factor with field may be seen in figure 3.1, where concentration factor is defined as (Internal Field)/(External Field).
It was found that the shell contruction of 36 MuMetal thin sheets gave the optimum concentration

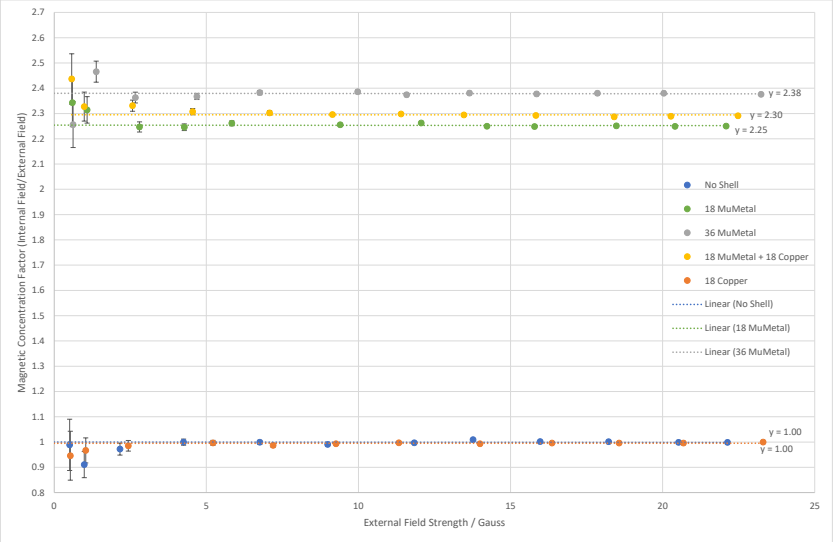

Figure 4. How concentration factor depends on frequency for a shell concentrating a static external field into its interior.

factor of $C = 2.38$ with minimal error (0.1%) at higher field strengths and a maximum error of 4.0% at an external field of 1.4 G. This increase in error at low magnetic fields is due to limited sensitivity of our Hall probe and current measurements over the Helmholtz coils.
Similar error relationships are observed for the other constructions. It should be noted that we assume the dipole has been placed in the same position and orientation in all experiments and so errors due to placement are excluded here.
It is expected that the copper will have no effect on a static magnetic field and this was confirmed by the 18 copper shell displaying no concentration of internal field. This is due to copper having a relative permeability similar to air, $\mu_r = 1.0$, and so negligible field guiding properties. In the oscillating magnetic field regime copper is expected to shield angular fields due to the production of eddy currents. Only air-gaps are used to block the angular component of a static magnetic field within our shells to simplify the experimental set up, however superconducting sheets in a similar shell have been shown to improve the concentration of static fields [**?**].

3.2. Power transfer

RL

Power is transferred from the primary circuit to a load resistor in the secondary circuit as explained in Methods XXX. This may be simply performed by placing a load resistor in parallel with the receiving inductor L_s forming an RL circuit as seen in XfX figure 2. To maximise power transferred, the optimal load resistance was matched to $R = \omega L$ (see Methods equation 8).
Figure 5 shows the relative PTE versus load resistance for various frequencies confirming the expected optimum load resistance of $R = \omega L$.
Mutual inductances between the coils at a set distance of 59 mm were found by measuring the voltage across the load resistor in the secondary RL circuit and the current driving the primary circuit. The copper only, MuMetal only, and full copper plus MuMetal shells all showed a concentrating effect by their relative increases in mutual inductance between the two coils as shown in the LHS of figure 6.

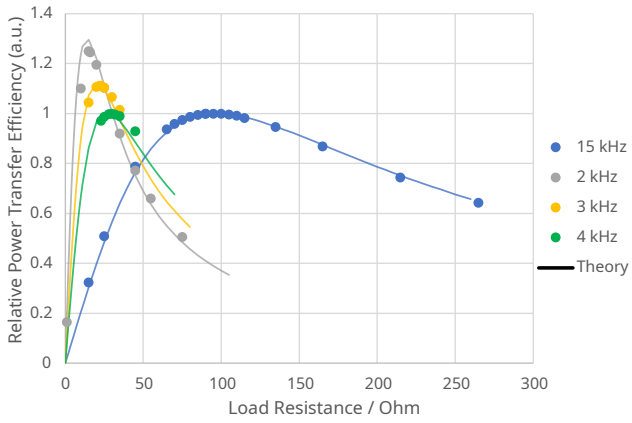

Figure 5.
Experimentally found relative power transfer efficiencies dependence on load resistance in a coupled RL inductive circuit for various frequencies. Theory line is found using equation 8.

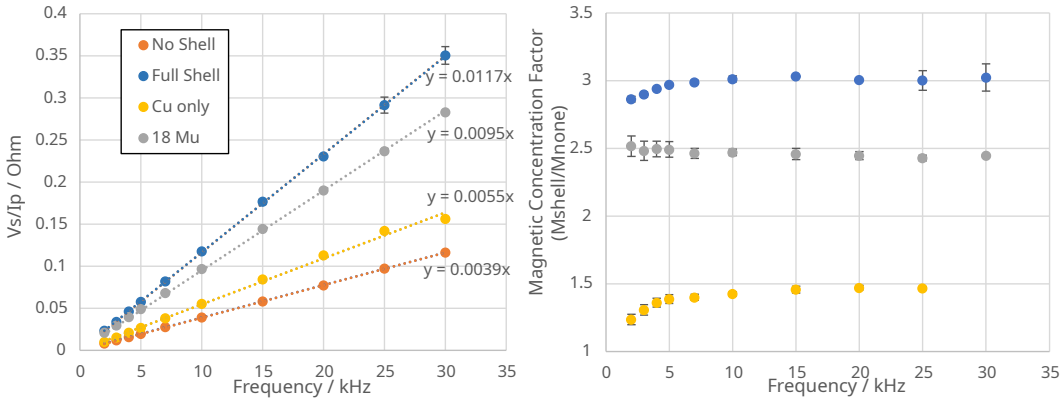

Figure 6. Exploring the behaviour of shells when the secondary receiving circuit is in the RL configuration. LHS: Finding mutual inductance, M, between two coils at a fixed distance for various shell configurations. The gradient is equivalent to $M/\sqrt{2}$ (equation 13). RHS: The shell's effect on mutual inductance is found by the ratio of (M with shell)/(M bare coil). An increase in mutual inductance corresponds to an increase in magnetic field density within the shell and is shown to be dependant on frequency for shells with copper present.

The full shell showed an increase of mutual inductance (magnetic field) by a factor of 3.0 ± 0.1. The frequency dependance on the relative increase in mutual inductance is shown on the RHS of figure 6. The two shell configurations containing copper are shown to have concentrating effects dependant on frequency. The concentrating effect rises steeply within the first 10 kHz and then plateaus for high frequencies. This expected behaviour initially motivated the choice for copper sheets in the shells for AC power transfer. At higher frequencies the perpendicular component of alternating magnetic fields produce eddy currents within the copper which, due to Lenz's law, oppose the change of field direction and effectively increases the angular permeability of the shell. Supporting work done on COMSOL (figure **??**) shows a similar observed effect where 36 copper sheets increases the concentration factor rapidly from $C = 1$ at 0 Hz to $C = 1.5$ (2SF) by 10 kHz and then only a small further increase in efficacy at higher frequencies.

Apart from errors due to instrument, measurement reading, and coil placement, we observed noise due to stray magnetic fields inducing pick-up within cables connecting the solenoid to the lock-in amplifier. This source of noise is highly frequency dependent and is at the same frequency as our desired signal, so could not be removed by the use of a lock-in amplifier. To supress this noise careful cable placement and shielding was installed.

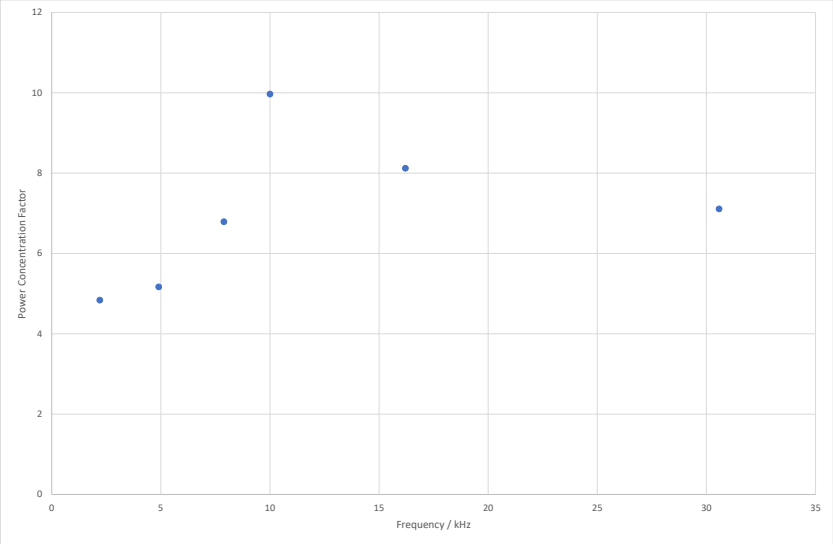

Figure 7. How the increase in power transfer efficiency depends on frequency in a coupled parallel RLC circuit.

Resonant — RLC

Parallel RLC circuits are more fitting for optimising power transfer [**?**]. For the arrangement described in figure 2 *b*, a shell comprised of 18 MuMetal and 18 Copper sheets was explored. The optimal load resistance was found by taking voltage measurements across a range of load resistance. An example power versus load resistance curve for 30 kHz can be seen in XXX figure **??**.
Optimal load resistances were found for a range of frequencies and PTE were calculated as shown in XXX figure **??**. Figure XX **??** shows the ratio of shell present versus no shell present for the range of frequencies. It can be seen that the increase of ratio between 0 and 10 Hz is still present, however due to the high error and few data points, other trends are hard to distinguish. In this arrangement, with the coils seperated by a distance of XXX mm, maximum observed power transfer is XX 0.05%. To further explore PTE, the distance between the two coils was varied. With a distance of XXX mm and a full shell around the receiving coil, a PTE of XXX% was achieved.
It was expected that a shell around the transmitting coil would further increase the field incident on the receiving coil. Therefore the arrangement described in Methods Figure **??** was constructed and the peak power transfer observed at 30510 kHz was found to be 1.01%.

Parallel RLC coupled to coil can be considered as figure 3.2. The voltage across R_{load} is equal to,

$$V_s = j\omega M I_p - j\omega L_s I_s.$$

I_s can be found by,

$$I_s = j\omega M I_p / z_s$$

where z_s is the total impedance of circuit 2...

$$V_s = \frac{MR}{L_s} I_p.$$

Therefore a plot of V_s/R against I_p will yield a gradient of M/L_s as seen in figure 3.2. Furthermore, $M = M(\omega)$ for shells with copper present, and so a plot of $(M/L_s)/(M^0/L_s^0)$ gives the relative in-

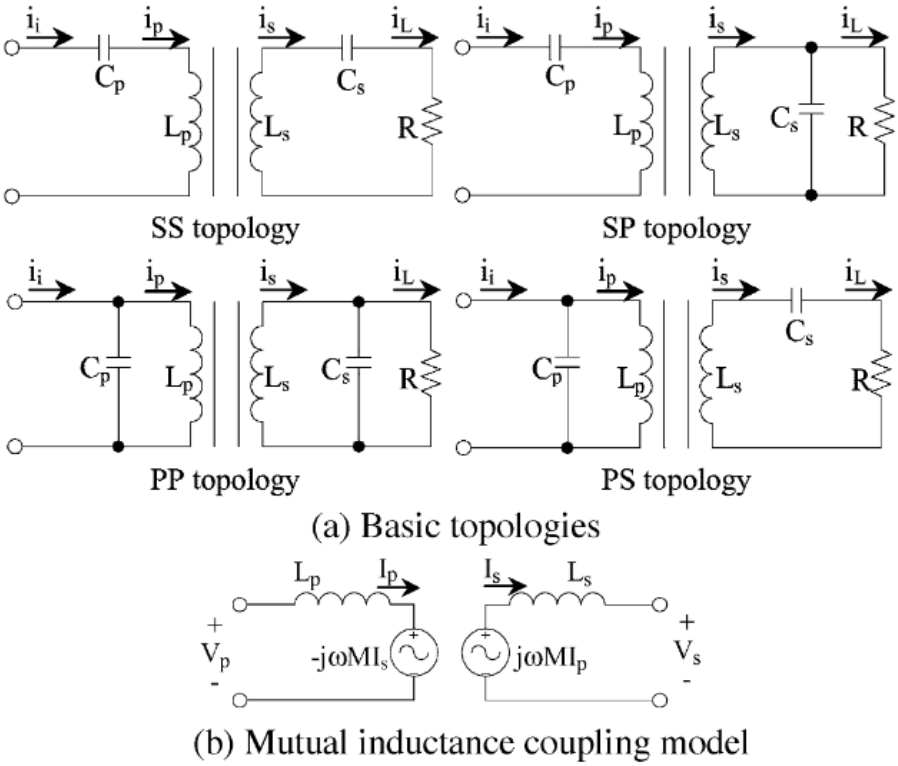

Figure 8.

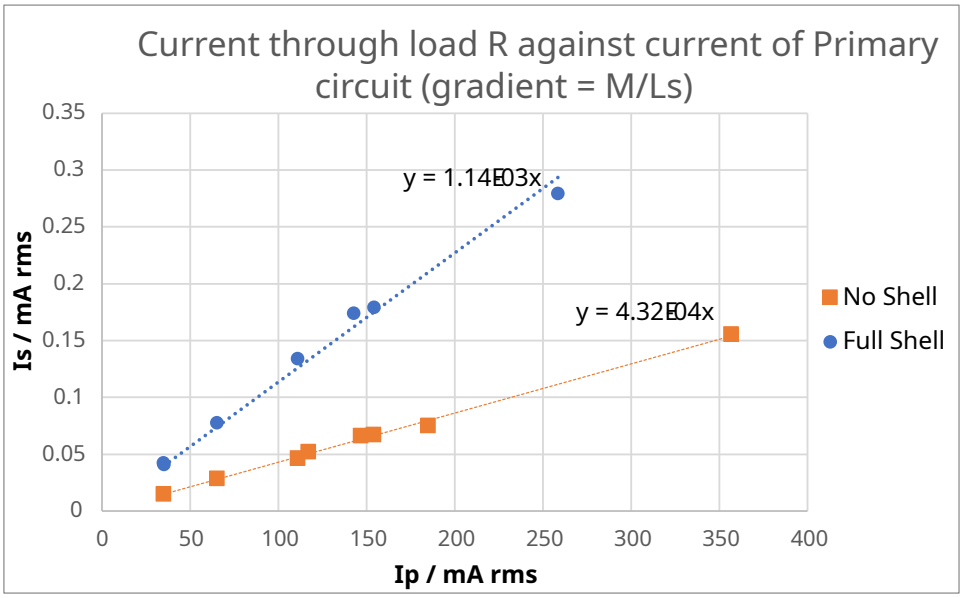

Figure 9.

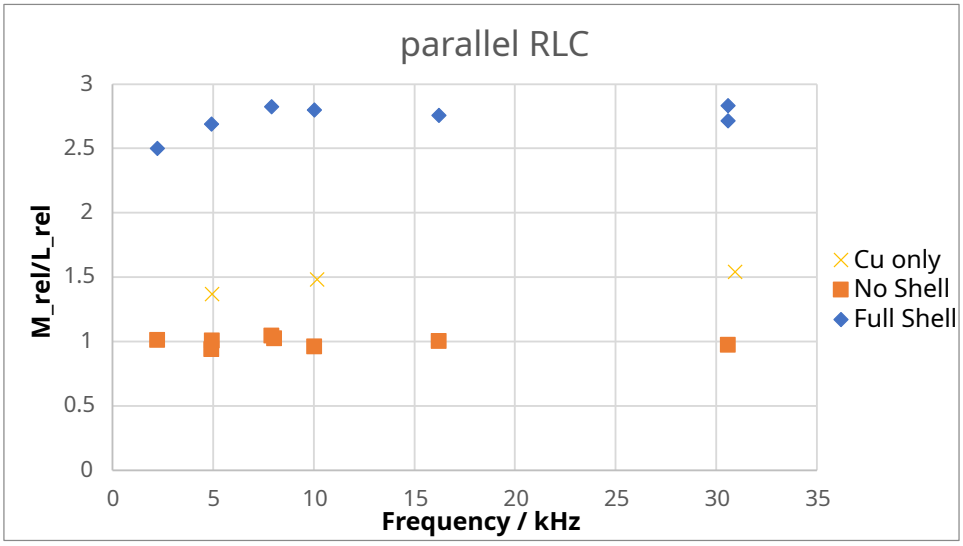

Figure 10.

crease in M/L_s with frequency as seen in figure 3.2.

3.3. Distance

Experimentally we found that power drops off as $r^{-5.6}$ which is in close agreement to the theoretical r^{-6}.

4. Discussion

For the constructed shells used in these experiments, their R_2/R_1 ratio was 40 ± 2 mm. From the theoretical TO work, it is predicted that the field should be concentrated by the perfect shell by R_2/R_1. We found a range of concentrations for both static, $C = 2.25 - 2.38$ XeX and oscillating, $C = 2 - 3.1$ XeX, external fields whose maximum concentration factors are still well below the expected theoretical concentration factor of 4.0 ± 0.2. This is likely explained by our approach to approximating the perfect TO designed anisotropic shells with shells comprised of discrete sections of high and low permeability. In both static and oscillating fields, we found that 36 MuMetal sheets performed better than 18 MuMetal sheets which suggests that finer discretization of the proposed shells gives concentrations closer to the theoretical value. In the static field experiments, only air was used to approximate the zero relative angular permeability. Air has a permeability of $\mu = 1$, which although is far less than the MuMetal's $\mu = XXX$, is likely still a poor approximation. This can be seen by the increase in performance in the oscillating external field experiments where copper sheets are introduced in order to effectively screen out angular field density by the production of Eddy currents. Eddy current screening is proportional to frequency of the oscillating field [**?**], and therefore, it can be seen that the concentration factor for shells with copper present increase with frequency.

Eddy currents may be modelled as a wire loop perpendicular to an oscillating magenetic field. A current is produced within the loop which is proportional to frequency of the field and, due to Lenz's law, flows in a direction to oppose the change in field density. The induced current in the loop is

$$I = \frac{A}{R}\omega(B - B'),$$

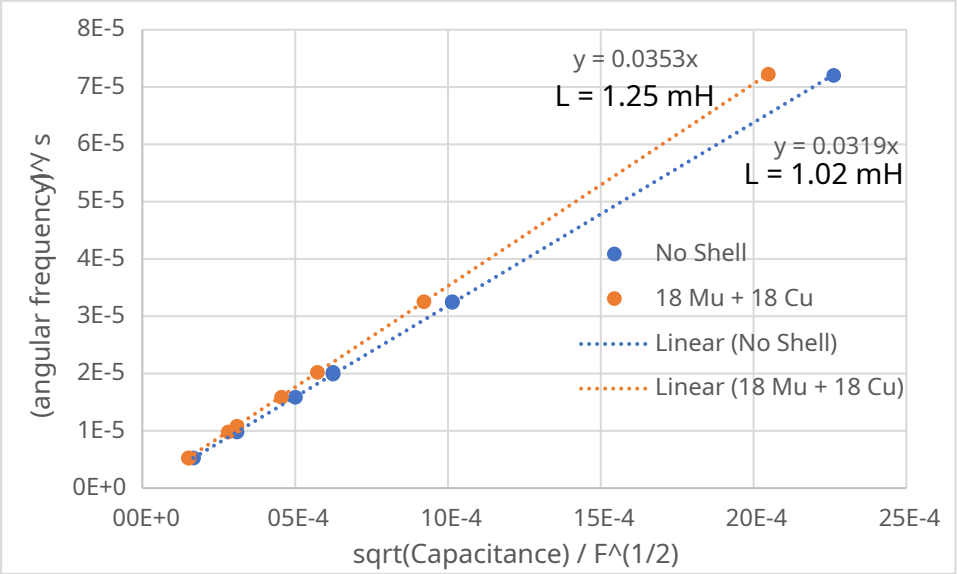

Figure 11.

and the field produced by the current is,

$$B' = -I\mu_0 r.$$

Combining these equations give,

$$B' = \frac{\omega B}{1+\omega},$$

which may be seen plotted with the COMSOL and experimental results for a copper only shell.

XwX Superconducting material has been suggested to effectively screen angular field in the static case [**?**]...

For many results we have assumed that the inductance of the solenoid was independent of the shell surrounding it. Here we shall reexplore some results without this assumption.
The resonant condition of a series RLC circuit,

$$\omega = 1/\sqrt{LC}, \tag{15}$$

allows the calculation of effective inductance L using the known capacitance, C and measured frequency peak, ω. Figure 11 shows ω^{-1} against $\sqrt{C}$ to find inductance L. The observed inductances for the two shell configurations are not sensitive to frequency however, it should be noted that the inductance of the coils used does have a dependency on current. For the range of currents used in the series RLC experiment, this change in inductance with current was negligible compared with the observed change in inductances with different surrounding shells. It was found that the inductance when surrounded by the full shell is 1.25 ± 0.01 mH whilst the bare solenoid and the copper only shell give an inductance of 1.02 ± 0.02 mH. This increase in inductance could be understood by the fact that the high permeability MuMetal in the shell is located near to the coil, increasing the relative permeability of space in the vicinity of the coil. From equation **??** it can be seen that the effective power concentration, η, for the RL circuit is dependent on both field concentration and effective inductance of the solenoid and in fact the increase in effective inductance reduces the increase in power transfer. The use of a tuned RLC setup within the receiving circuit can counteract this loss of power concentration with increased inductance as the load resistance no longer needs to match ωL,

as discussed in Methods.

Due to the sharp drop off of power transfer with distance, the greatest PTE found was 1.01% XeX at a seperation of 48.7 mm with both the transmitting and receiving coil surrounded by a concentrating shell. The reason for this poor efficiency is largely due to the non-ideal real resistive component of the transmitting coil.

DC:
- further explanation on error source in placement

Linear decay of coil in non RLC
- Due to pick up that is proportional to w^2?
- Expected drop off due to magnetic saturation? or other reasons for MuMetal failure. - COMSOL MU thickness

Power transfer
- Generally low PTE due to high loss of inductor. Could have used laminated AC inductor to reduce eddie currents. Could have not used iron core as hysteresis.
- Discussion of other power transfer techniques and coupled inductor papers. Why a shell is better than no shell with distances.
- Why a shell allows a small radii inductor to be used - efficiency of scale Better coupling for given distance. See p.51 pratt.
- Relationship of PTE with distance -$r^{-5.6}$. Effective mutual inductance changed.
- Two shells present.
- Another exploration on error sources and summary of largest sources.

Comparison of RL, series RLC and parallel RLC circuitary:
- models
- expected efficiency

can use a smaller solenoid, plot spider graphs in python

5. Conclusions

EXTENSIONS
0) For further understanding we would need to look at more frequencies and expecially at much higher freqs. A selection of different dipoles would also be beneficial to ensure that frequency dependence is not linked to non-ideal dipole.

0) Perhaps another circuit could be designed that works more similarly to an RLC? Could propose one however experimentation has not been performed.

0) Could a more complicated and directional shell be designed for power transfer?

6. References